International Forum on Aeroelasticity and Structural Dynamics
IFASD 2019
9-13 June 2019, Savannah, Georgia, USA

NUMERICAL INVESTIGATION OF UNSTEADY TRANSITIONAL BOUNDARY LAYER FLOWS

Michael Fehrs[1], **Sebastian Helm**[1], **Christoph Kaiser**[1]

[1] DLR - German Aerospace Center
Institute of Aeroelasticity
Bunsenstraße 10, 37073 Göttingen, Germany
Michael.Fehrs@dlr.de

Keywords: unsteady boundary layer transition, transition modeling, unsteady aerodynamics, airfoil flutter

Abstract: Different numerical models are available for the prediction of laminar-turbulent transition in boundary layer flows. Although these models gained some maturity in the application for steady flows, little is known about the applicability for unsteady problems in a broad frequency and Reynolds number range. This paper will investigate different unsteady transition prediction methods in external aerodynamics. Flow conditions are identified that unambiguously require an unsteady transition prediction and such that are likely to be covered by a quasi-steady approach. This will help to outline the requirements for future unsteady transition models and to trace deficiencies of existing methods.

1 INTRODUCTION

Boundary layer transition is the process in which a laminar boundary layer changes into a turbulent state. A boundary layer flow that undergoes transition at some point will be called *transitional*. Laminar flow is often discussed in terms of a possible drag reduction by some active or passive means. However, the transitional flow affects forces acting on airfoils and wings in a much more fundamental way: as the laminar part of the boundary layer flow reduces the displacement thickness of the boundary layer at the trailing edge, the effective camber of the device and the lift and moment are changed.

An example of this effect on the pressure distribution is shown in Fig. 1 for a NACA0012 airfoil at $\alpha = 1^\circ$ obtained with computational fluid dynamics (CFD). The transition locations for both cases are imposed in the CFD computation. As the transition location on the upper side of the airfoil moves downstream, the displacement thickness is reduced. On the lower side, the opposite effect can be observed. The overall displacement of the flow given by the airfoil and the displacement thickness of the boundary layer is changed and the difference in effective camber results in a different pressure distribution.

Although the displacement thickness and the relative difference between a transitional and a fully turbulent boundary layer decreases with increasing Reynolds number, differences in the lift and moment characteristics of an airfoil or wing are still found. This is especially true for transonic flow conditions, where the difference in boundary layer displacement changes the shock location and strength [1].

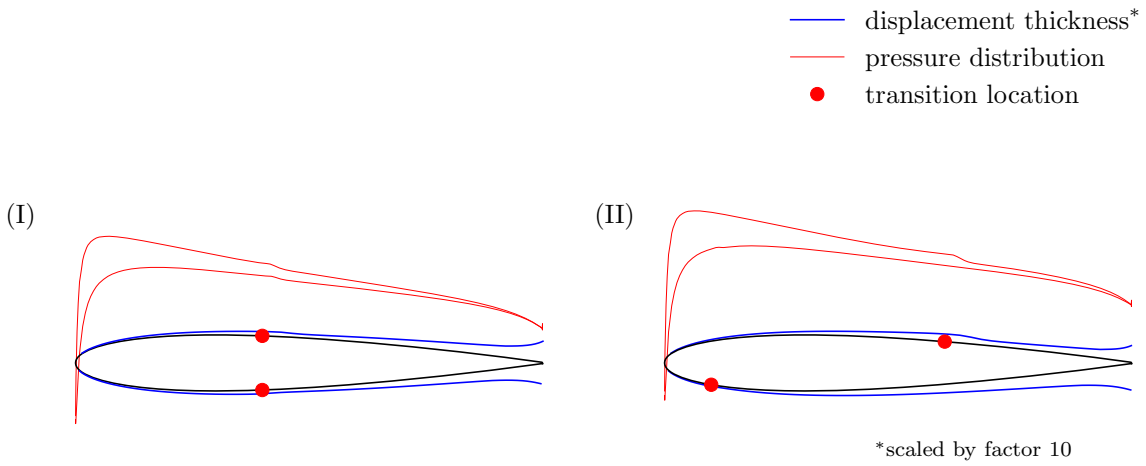

Figure 1: Displacement thickness for different transition locations and the effect on the pressure distribution.

The different aerodynamic characteristics of transitional flows influence the aeroelastic behavior which in turn needs to be reliably assessed. Although transitional effects are expected to be less significant at free-flight Reynolds numbers than at moderate wind tunnel Reynolds numbers, they have to be treated with the same degree of confidence as done for fully turbulent flow conditions [2].

At the moment, there is a lack of genuine unsteady transition models as most available models are based on steady flow assumptions. These models are usually applied to unsteady flow conditions, leading to a quasi-steady approach. In addition, experience is sparse on how different transition models behave in a broad frequency band, Mach number, and Reynolds number range. Fehrs [1] and Helm et al. [3] observe that correlation-based models with free boundary layer transition give similar results as computations with a constant transition location at small excitation amplitudes and free-flight Reynolds numbers in unsteady flow. This indicates that a threshold Reynolds number may exist for which no unsteady transition prediction is required for an aeroelastic assessment. This paper is meant to improve the understanding of transition model behavior in the framework of dynamic stability problems.

The next section describes the methods used to obtain the aerodynamic data required for flutter computations of airfoils with free boundary layer transition. The third section presents steady and unsteady aerodynamic data for boundary layer flows with free transition and results obtained with a novel frozen transition approach described in the second section. The last section draws the conclusion of this paper.

2 METHODS

2.1 CFD-based Unsteady Aerodynamics

Unsteady aerodynamics includes a broad variety of different time-depending flow conditions. The temporal changes in flow conditions might be periodic in nature (e.g. wake encounter in turbomachinery) or a discret event (e.g. gust encounter). This article will focus on motion induced, harmonic forces as they are required for stability analysis.

Stability is the quality of being immune to small disturbances [4]. Therefore it is sufficient to determine if a system is stable by addressing small departures from the static state. These may be an excitation in the pitch or heave degree of freedom of an airfoil. The aerodynamic response to these disturbances determines if the system encounters, for example, flutter. The general form of the flutter equation is given by [5]:

$$\left[\frac{U^2}{c^2}\,[M]\,p^2 + [K] - \frac{1}{2}\rho\,U^2\,[A(p)]\right]\{q\} = 0 \tag{1}$$

with the eigenvalue[1] $p = \delta + ik$ describing the reduced damping and reduced frequency of the system, the freestream velocity U, the chord length c, and density ρ. The reduced frequency is given by:

$$k = \frac{c\,\omega}{2\,U} \tag{2}$$

The vector $\{q\}$ describes the generalized coordinates. The inertia $[M]$ and stiffness $[K]$ matrices define the structure of the system. For harmonic motion, it is assumed that the aerodynamic matrix is a function of reduced frequency k: $[A(ik)]$. In the case of an airfoil with heave and pitch degrees of freedom, the aerodynamic matrix is given by the derivatives of the aerodynamic coefficients:

$$[A(ik)] = \begin{bmatrix} -c_{lh}(ik)\,S & -c_{l\alpha}(ik)\,S \\ c_{mh}(ik)\,Sc & c_{m\alpha}(ik)\,Sc \end{bmatrix} = \begin{bmatrix} -\frac{\partial c_l}{\partial h}(ik)\,S & -\frac{\partial c_l}{\partial \alpha}(ik)\,S \\ \frac{\partial c_m}{\partial h}(ik)\,Sc & \frac{\partial c_m}{\partial \alpha}(ik)\,Sc \end{bmatrix}, \tag{3}$$

where the unsteady aerodynamic coefficients c_{lh}, $c_{l\alpha}$, c_{mh}, $c_{m\alpha}$ are complex-valued functions[2] of reduced frequency k and S is a reference area. In general, there is no explicit function to describe the frequency-dependent aerodynamic matrix. Therefore, $[A(ik)]$ needs to be determined at discret values of k.

One way to obtain $[A(ik)]$ is to rely on time-domain CFD computations and afterwards obtaining the transfer function $G(ik)$ given by the Fourier-transformed system response $Y(ik)$ and excitation $U(ik)$:

$$G(ik) = \frac{Y(ik)}{U(ik)}, \tag{4}$$

where e.g. $G(ik) = c_{l\alpha}(ik) = \mathrm{FFT}\{c_l(t)\}/\mathrm{FFT}\{\alpha(t)\}$ for pitch motion of a specific reduced frequency k. An example of the unsteady forces acting on an airfoil during a mono-frequent, forced motion pitch excitation[3] is given in Fig. 2.

[1] Assuming e.g. the p-k method by Hassig [5].

[2] The moment reference axis is about quarter-chord for all data given in this paper. For all pitch computations in this paper, a rotation about the quarter-chord position is used.

[3] The overbars denote mean value.

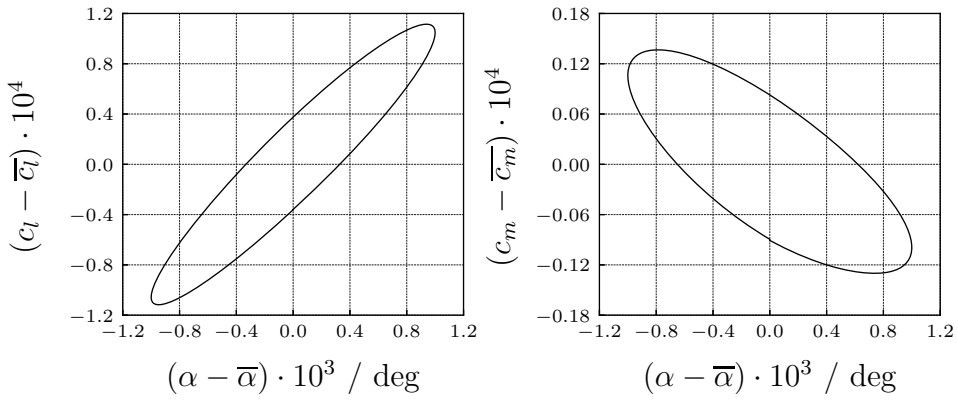

Figure 2: Forced pitch motion computation at a single frequency.

More straightforward than the mono-frequent approach is the use of linear system identification techniques, for which a broadband pulse excitation is used to obtain the frequency response of the system for a certain frequency band [6]. The fundamental frequency f depends on the number of time steps N computed and the time step size Δt:

$$f = \frac{1}{T} = 1/\sum_{n=1}^{N} \Delta t \tag{5}$$

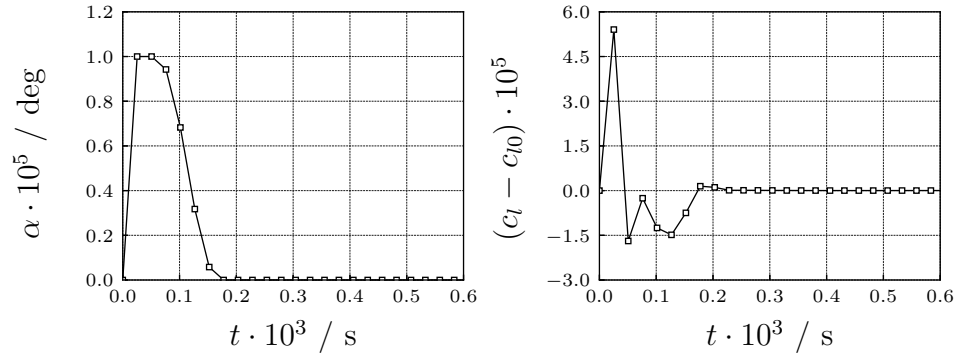

Figure 3: Pulse computation for a pitch excitation.

The system response c_l is corrected by the lift coefficient time series of a second computation without excitation c_{l0} to remove any drift in the unsteady solution. An example of a pulse excitation of the angle of attack and the corrected lift response $c_l - c_{l0}$ is shown in Fig. 3.

In order to obtain a linear response of the system with any of the two approaches, the excitation needs to be sufficiently small. Figure 4 depicts the effect of excitation amplitude $\hat{\alpha}$ on the magnitude of the unsteady moment coefficient derivative $|c_{m\alpha}|$. The unsteady aerodynamics converges towards the amplitude independent value for sufficient small excitation amplitudes. A converged system response in transonic airfoil flows is usually found for amplitudes $\hat{\alpha} \leq 1^\circ \cdot 10^{-4}$.

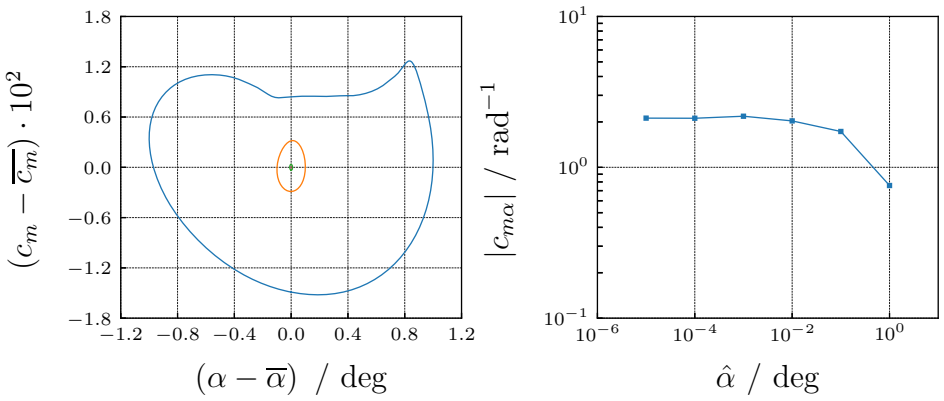

Figure 4: Influence of excitation amplitudes $\hat{\alpha}$ on the magnitude of the unsteady aerodynamic moment coeffcient derivative $|c_{m\alpha}|$.

2.2 Transition Prediction

2.2.1 Free Transition

Different methods exist in a Reynolds-averaged Navier-Stokes (RANS) framework to predict the transition location that is freely determined by the specific flow conditions. The most known is the e^N method independently developed by van Ingen [7] and Smith & Gamberoni [8], where the stability of the boundary layer flow with respect to small disturbances is investigated for local velocity profiles inside the boundary layer. The amplification rates α_i are integrated along the body to obtain the amplification factor $n = \int_{x_0}^{x} \alpha_i \, dx$, which is compared to a critical N factor [9].

The critical N factor needs to be determined by experiments for different wind tunnel or flight conditions. Therefore, the method is considered semi-empirical. The method requires non-local quantities (velocity profiles, integral quantities), which requires some additional data handling. Highly sophisticated implementations of the e^N method exist and it has become the standard method in the aircraft industry [10, 11].

In recent years, correlation-based local transition models have gained more attention, especially the γ-Re_θ transition model, for which the strictly local formulation allows a straightforward use in modern CFD codes [12–14]. A comprehensive overview about correlation-based transition models is given by Dick & Kubacki [15].

The γ-Re_θ transition model correlates the momentum loss thickness Reynolds number at transition onset $Re_{\theta t}$ to the local turbulence level and streamwise pressure gradient. The actual momentum loss thickness Reynolds number Re_θ is approximated by the locally defined vorticity Reynolds number Re_ν to determine the transition onset. Fehrs [1] proposes a simplified version of the γ-Re_θ model solely based on the γ transport equation and therefore named γ transition model. The model is specifically designed for Tollmien-Schlichting transition in external flows in a low turbulence environment and improves the correlation for accelerated boundary layer flows. The γ transition model is used for all free transition computations in this article.

Besides the differences between the transition prediction methods, all models mentioned above are coupled to the underlying turbulence model in a similar manner: when a laminar flow region is identified, the turbulence production is disabled, which results in a laminar boundary

layer flow as $\mu_t \rightarrow 0$. However, the blending used to increase the turbulence kinetic energy downstream of the transition location is different.

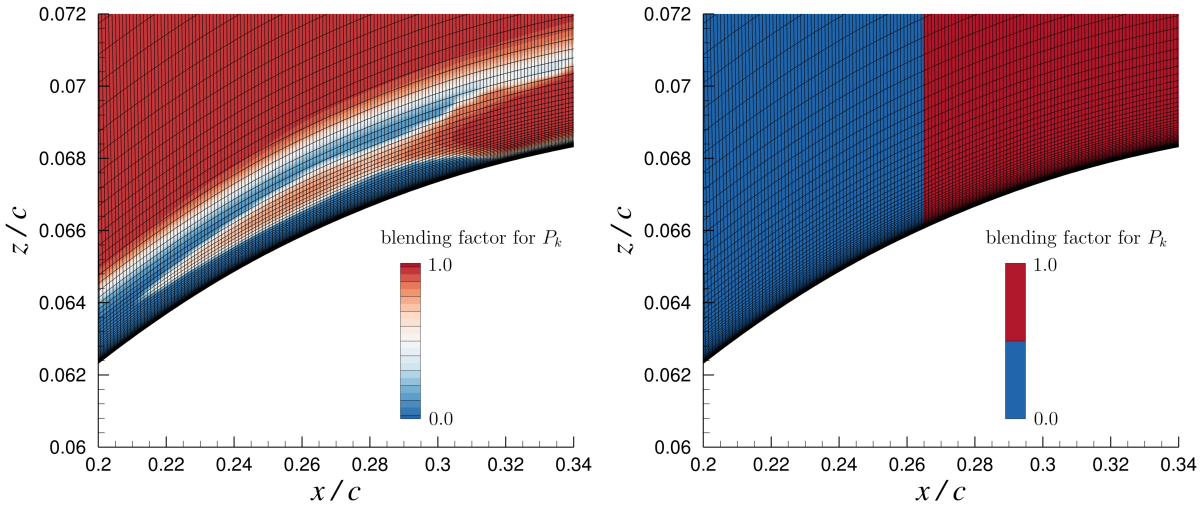

Figure 5: CAST10-2: Difference in blending between γ transition model (left) and TAU transition module (right).

The DLR TAU-Code transition module provides an e^N method implementation, where no specific blending is used. The full turbulence kinetic energy production term P_k is enabled downstream of the transition location. This behavior is shown on the right of Fig. 5. In the γ-Re_θ and γ transition model, the intermittency variable γ is used within an additional transport equation to increase the turbulence kinetic energy production over a certain distance[4]: $\widetilde{P}_k = \gamma\, P_k$. This leads to a smooth blending from the laminar to the turbulent boundary layer as shown on the left of Fig. 5.

In addition, the γ model approximates the thickness of the laminar boundary layer to preserve the turbulence model characteristics in the freestream. In the TAU transition module (e^N method), the production term is disabled up to a user specified wall-normal distance.

The TAU transition module sets the transition location to the surface grid points closest to the location specified by the user or found by the stability analysis. Therefore, the method is more sensitive to the grid resolution at the transition location. Although the transition onset (e.g. first intermittency increase) found by the γ model is also started at some grid point, the model blending allows for a more sensitive and smoother reaction to changes in the flow conditions.

Fehrs [1] shows that the TAU transition module (e^N method) applied for transition prediction at $Re = 20 \cdot 10^6$ gives no variation of the transition location for a pitching airfoil with a pitch amplitude of $\hat{\alpha} = 1^\circ \cdot 10^{-4}$. The grid has a constant cell length of $\Delta x/c = 0.002$. To obtain an unsteady motion of the transition location, a local grid refinement is required, which is not a viable option if many different flow states within the flight envelope are considered.

The unsteady aerodynamics obtained with the TAU transition module for these cases are identical to results predicted by the γ transition model for which the intermittency distribution reacts to the unsteady flow field. The same behavior is reported by Helm et al. [3] for airfoil sections of the DLR-F5 wing at high Reynolds numbers. For these specific cases, there is no additional

[4]It should be noted that in the laminar flow region the minimum blending factor is $\gamma = 0.02$.

benefit by using the available transition prediction in an unsteady computation as the unsteady intermittency field (γ transition model) results in the same aerodynamics as the constant transition location (TAU transition module, e^N method).

2.2.2 Frozen Transition Location

Frozen transition location will denote a flow state in an unsteady CFD computation, for which the transition location and the blending to turbulence does not change in time. The DLR TAU-Code transition module allows to impose a user-defined transition location independently of the actual flow, which can be used to model a boundary layer tripping in a steady computation. The consideration of the boundary layer tripping improves the agreement between numerical and experimental data significantly [16].

2.2.3 Frozen Intermittency

Frozen intermittency will denote a flow state in an unsteady CFD computation, for which the intermittency field does not change in time. The intermittency field is determined by a steady computation with the γ transition model for given flow conditions. At the moment it is not possible to specify an arbitrary transition location like it is possible with the TAU transition module.

3 RESULTS

3.1 Overview

Steady and unsteady results for three different airfoils at different flow conditions are presented in this section. The test cases include a transonic flow at a moderate Reynolds number (CAST10-2), subsonic flows at moderate to high Reynolds numbers (NLF1-0414F), and transonic flows at moderate to high Reynolds numbers (SC(2)-0012).

Steady results with free boundary layer transition are obtained in some angle of attack range with the γ transition model. One angle of attack is chosen for further unsteady computations. For this angle of attack, the TAU transition model is used to impose a transition location that gives a good approximation of the transition location predicted by the γ model. The imposed transition location is afterwards used in an unsteady computation as a frozen transition location. The results are compared to unsteady computations with free boundary layer transition as predited by the γ transition model. For some cases, the frozen intermittency approach is used as well.

3.2 CAST10-2: Transonic Flow at a moderate Reynolds number

3.2.1 CAST10-2: Airfoil Description

The CAST10-2 supercritical airfoil is part of a family of airfoils designed for a transonic commercial transport aircraft. The design point of the airfoil is given at $M = 0.76$, $\alpha = 0.2^\circ$ with $c_l = 0.595$ [17]. The section coordinates are given by Dress et al. [18], see Fig. 6. The DLR projects *IGREEN* [19] and *ALLEGRA* [20–23] provide experimental and numerical data on the aerodynamics and flutter stability of the CAST10-2 in transonic flow. Investigations on limit cycle oscillations and flutter occurring at transonic flow conditions are presented by Braune & Hebler [24]. Braune & Hebler [25] provide a further analysis of the single-degree-of-freedom flutter observed for the CAST10-2 at these transonic flow conditions.

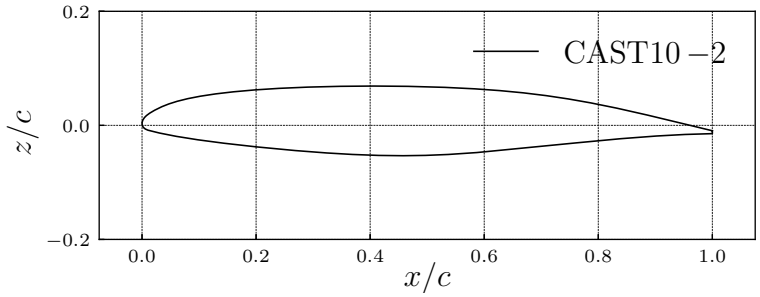

Figure 6: CAST10-2: Geometry.

3.2.2 CAST10-2: Steady Results

The CAST10-2 airofil is investigated at a Reynolds number of $Re = 2 \cdot 10^6$ and Mach number $M = 0.73$ at an angle of attack at the upper bound of the laminar drag bucket. Braune & Hebler [24] provide experimental data that allows an assessment of the transition model capabilities for the given flow conditions. Figure 7 depicts the aerodynamic coefficients computed with the γ transition model and the experimental data of Braune & Hebler [24] for different angles of attack α. The root mean square (rms) errors of the aerodynamic coefficients are included for the experimental data.

The grey shaded area in the CFD data marks flow conditions, for which the steady solver does not converge. The flow is inherently unsteady for these angles of attack with a periodic development of flow separations and shocks on the upper surface of the airfoil. The shaded area is limited by the instantaneous maximum values of the unsteady aerodynamic coefficients. Wind tunnel walls and model deformations are not considered in the numerical model, which accounts for some of the off-set between experiment and numerical values. The overall agreement is reasonably well as the lift, drag, and moment curves are qualitatively reproduced by the γ transition model.

Figure 8 depicts the pressure c_p and skin friction c_f coefficient distributions for $\alpha = 0°$ for a free transition computation and the result given by an imposed transition location defined by the TAU transition module. In both cases, the flow is transonic with a weak shock at the transition location. Transition is set to $x/c = 0.265$ on the upper and to $x/c = 0.56$ on the lower surface, which gives the best agreement with the free transition case. It takes about 10 % of the chord length to activate the turbulence production over the full height of the boundary layer for the γ model compared to the sudden increase given by the TAU transition module[5]. As a result, it is not possible to match the exact increase in skin friction as the blending differs.

In addition, γ model results for $\alpha = [-0.1°, -0.05°, 0.05°, 0.1°]$ are depicted by gray lines in Fig. 8 to demonstrate the change of transition location[6] with angle of attack. In order to analyse the effect of the transition location on the steady aerodynamics further, these angles of attack are computed with a frozen transition location given by the imposed location for $\alpha = 0°$ and a frozen intermittency field given by the intermittency field for $\alpha = 0°$.

The resulting aerodynamic coefficients are shown in Fig. 9. Although the pressure distribution indicates a good agreement for the free and frozen computations at $\alpha = 0°$, the quasi-steady

[5]The blending between the laminar and turbulent boundary layer for this case is depicted in Fig. 5.
[6]Given by the main increase in c_f.

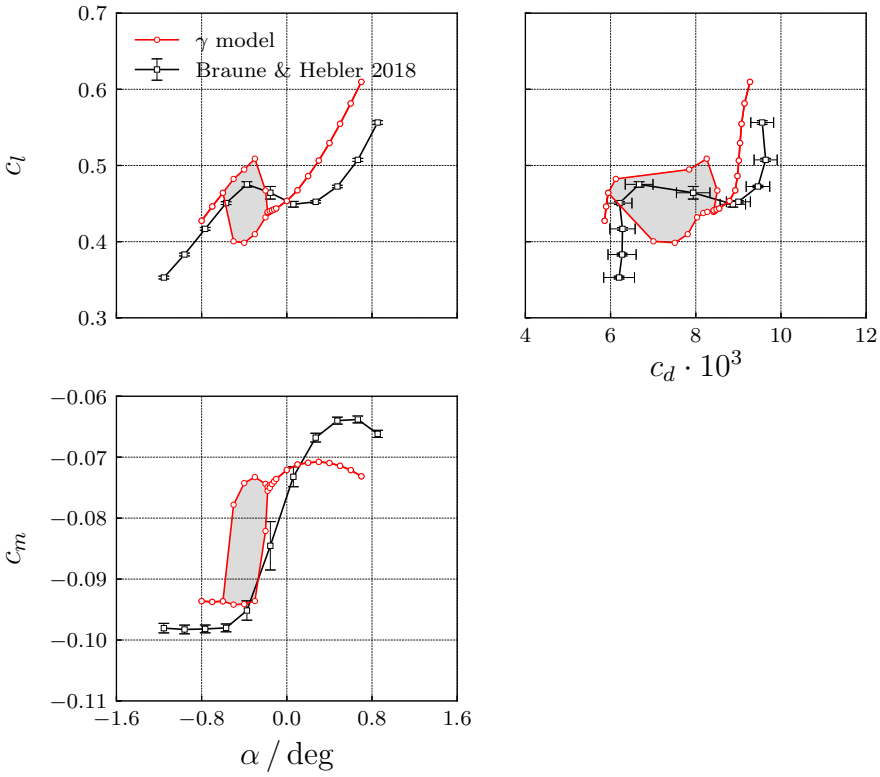

Figure 7: CAST10-2: Aerodynamic coefficients at $Re = 2 \cdot 10^6$, $M = 0.73$.

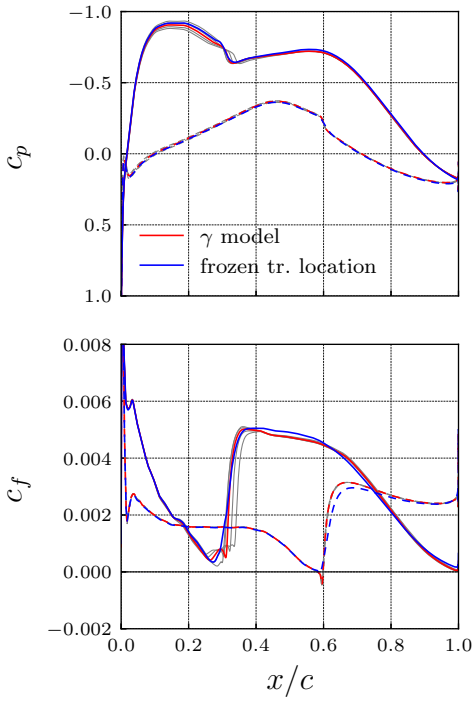

Figure 8: CAST10-2: Approximation of free transition (γ model) results by an imposed transition location (frozen tr. location) at $\alpha = 0°$. The gray lines show γ model results for $\alpha = [-0.1°, -0.05°, 0.05°, 0.1°]$.

derivatives are significantly different in magnitude, which already shows the importance of a free transition prediction for these flow conditions.

Table 1: CAST10-2: Quasi-steady lift and moment coefficient derivatives at $\alpha = 0°$ obtained with central differences.

	$\Delta c_l \,/\, \Delta\alpha \,/$ rad^{-1}	$\Delta c_m \,/\, \Delta\alpha \,/$ rad^{-1}
γ model	6.56	0.720
frozen intermittency	9.12	0.362
frozen tr. location	8.96	0.320

Table 1 gives the quasi-steady lift and moment coefficient derivatives at $\alpha = 0°$ obtained with central differences. Both frozen transition approaches give similar results but differ significantly from the free transition case. Therefore, the change of transition position with angle of attack is more important than the blending from laminar to turbulent.

3.2.3 CAST10-2: Unsteady Results

A pulse excitation with a pitch amplitude of $\hat{\alpha} = 1° \cdot 10^{-5}$ is used to determine the unsteady aerodynamics at a mean angle of attack of $\overline{\alpha} = 0°$. Figure 10 shows the lift coefficient derivative $c_{l\alpha}$ and the moment coefficient derivative $c_{m\alpha}$ in magnitude and phase against reduced frequency k.

The difference in the quasi-steady gradients shown in Sec. 3.2.2 are present at $k = 0$. The free transition results show aerodynamic resonance peaks, which are found neither for the frozen transition location nor for the frozen intermittency case. Mono-frequent computations are used to confirm the resonance behavior. All results are similar for reduced frequencies of $k > 0.5$. For these high reduced frequencies, the unsteady aerodynamics is determined by non-circulatory forces, for which the overall displacement of fluid caused by the airfoil and the boundary layer are similar for all cases considered.

Figures 11 and 12 depict the local unsteady pressure $c_{p\alpha} = \partial c_p/\partial\alpha$ and skin friction $c_{f\alpha} = \partial c_f/\partial\alpha$ coefficient distributions for $k = 0.25$ and $k = 0.45$ in magnitude and phase against chord length[7]. The main resonance peak in the unsteady moment coefficient $c_{m\alpha}$ occurs at $k = 0.45$.

The difference in unsteady loads at $k = 0.45$ is caused by the oscillation of the shock position and transition location on the upper surface, mainly affecting the downstream pressure distribution. The effect is strongest for the free transition case predicted by the γ transition model. For $k = 0.25$, the magnitude of the unsteady pressure $|c_{p\alpha}|$ at the transition location decreases. The upstream pressure distribution is mainly affected by the shock-wave/boundary layer interaction at this reduced frequency. All cases show a qualitatively similar behavior in phase. An inverse shock motion is found at $k = 0.45$ and a regular shock motion at $k = 0.25$.

[7]The dimensional frequencies are $f = 19.25$ Hz at k = 0.25 and $f = 34.65$ Hz at $k = 0.45$.

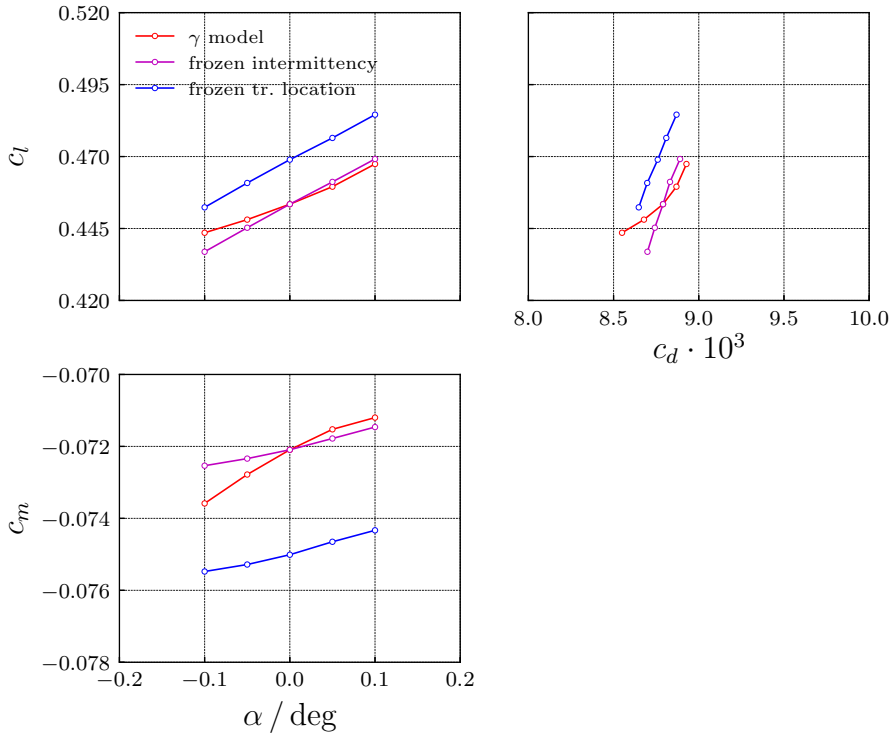

Figure 9: CAST10-2: Aerodynamic coefficients with free transition, frozen transition location, and frozen intermittency.

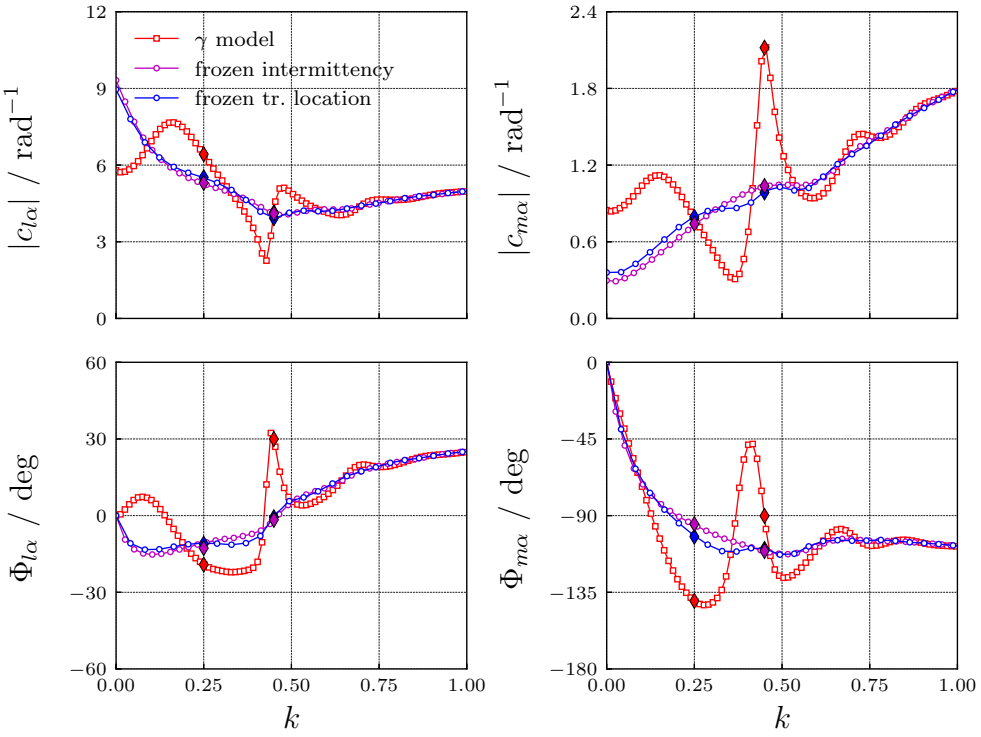

Figure 10: CAST10-2: Unsteady aerodynamic derivatives with free transition, frozen transition location, and frozen intermittency for a pulse excitation. Diamonds indicate mono-frequent results.

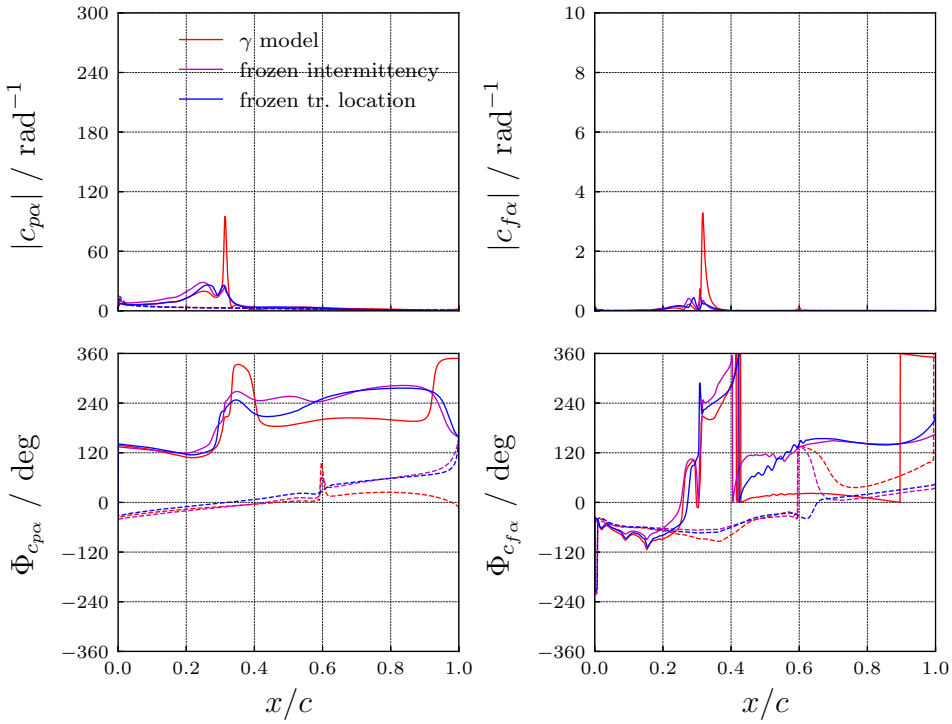

Figure 11: CAST10-2: Unsteady pressure $c_{p\alpha} = \partial c_p/\partial\alpha$ and skin friction $c_{f\alpha} = \partial c_f/\partial\alpha$ coefficient distribution at $k = 0.25$. Dashed lines depict lower surface.

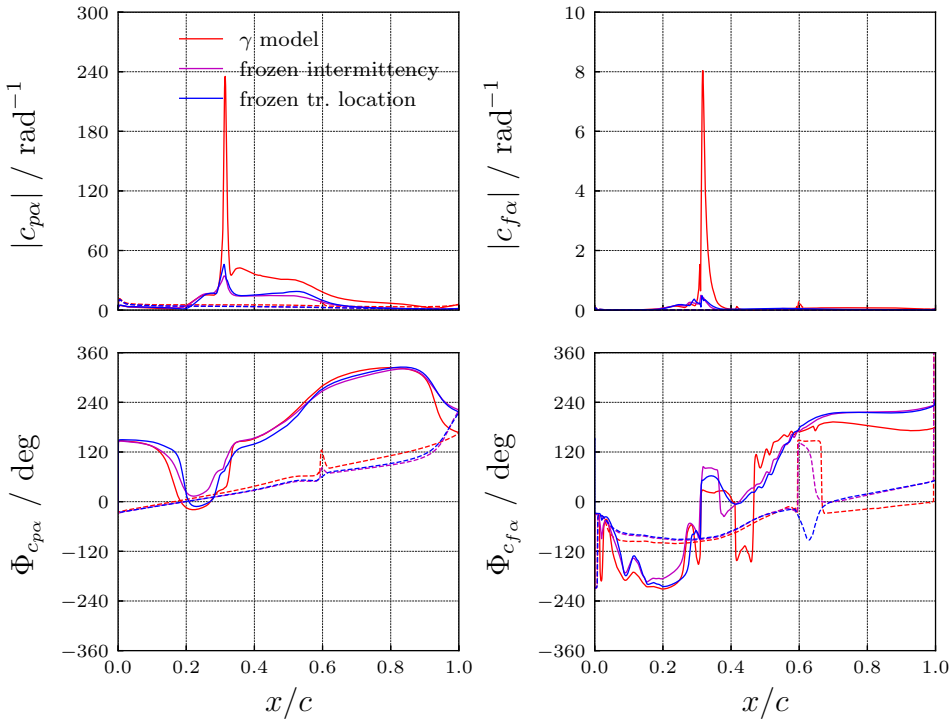

Figure 12: CAST10-2: Unsteady pressure $c_{p\alpha} = \partial c_p/\partial\alpha$ and skin friction $c_{f\alpha} = \partial c_f/\partial\alpha$ coefficient distribution at $k = 0.45$. Dashed lines depict lower surface.

3.3 NLF1-0414F: Subsonic Flows at moderate to high Reynolds numbers

3.3.1 NLF1-0414F: Airfoil Description

In this section, the NLF1-0414F airfoil is used to investigate the unsteady transition behavior in subsonic flow. The airfoil is designed for lift coefficients of $c_l = 0.4$ to 0.45 at $Re = 10 \cdot 10^6$ and $M \leq 0.4$ [26]. It is shown in Fig. 13. Fehrs [1] uses the wind tunnel data of McGhee et al. [26] to validate the γ transition model in a Mach number range of $M = 0.05$ to 0.4 at low to moderate Reynolds numbers of $Re = 3 \cdot 10^6$ to $10 \cdot 10^6$. It is found that the extent of the laminar drag bucket is predicted reasonably well.

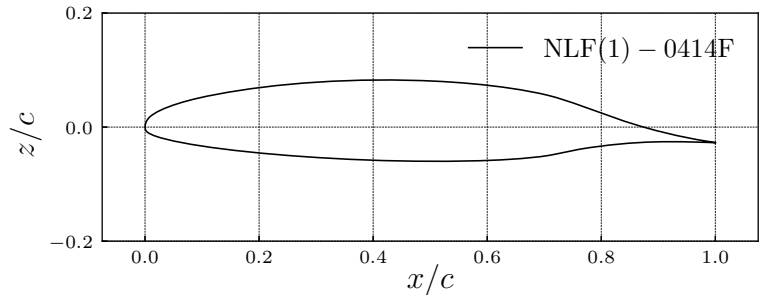

Figure 13: NLF1-0414F: Geometry.

3.3.2 NLF1-0414F: Steady Results

The steady flow field around the NLF1-0414F airfoil is computed at different Reynolds numbers at $M = 0.3$ with the γ transition model. The results in terms of aerodynamic coefficients for $Re = 2 \cdot 10^6$, $10 \cdot 10^6$, and $20 \cdot 10^6$ are presented in Fig. 14. As the Reynolds number increases, the extent of the laminar drag bucket decreases. The lowest drag coefficients are found for the design Reynolds number of $Re = 10 \cdot 10^6$. The quasi-steady lift and moment curve slope inside the laminar drag bucket is similar for all Reynolds numbers.

The transition location at $\alpha = -1^\circ$ given by the γ transition model is approximated by imposing a transition location with the TAU transition module. Figure 15 shows the approximation in terms of pressure c_p and skin friction c_f coefficients. The agreement is best for high Reynolds numbers. At $Re = 2 \cdot 10^6$ transition takes place over a large laminar separation bubble on the upper surface. The friction coefficient distribution indicates that the imposed transition location needs to be moved further downstream. However, moving the transition location further downstream results in an unsteady flow condition. The approximation by the TAU transition module is worst for this Reynolds number.

The imposed transition locations for $\alpha = -1^\circ$ are kept and the angle of attack is slightly varied. The results are depicted in Fig. 16. The agreement of the values of lift and moment coefficients together with the slope of the curves is best for $Re = 10 \cdot 10^6$, indicating that the transition location is independent of the angle of attack. As shown in Fig. 15, transition takes place downstream of the pressure minimum over a small laminar separation bubble. As the location of the pressure minimum is rather insensitive to small changes in the angle of attack, this turns out in a stable transition location.

At $Re = 20 \cdot 10^6$ transition takes place in a favorable pressure gradient region. Any change in angle of attack will change the pressure gradient, directly affecting the transition location and thus causing a larger difference between the free and imposed transition results than for $Re = 10 \cdot 10^6$.

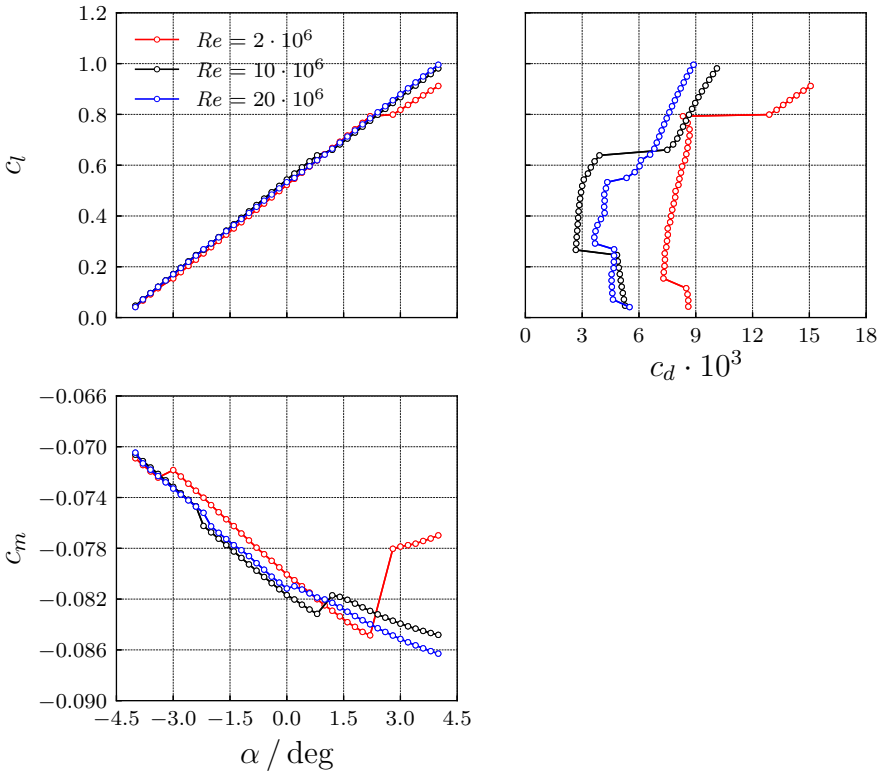

Figure 14: NLF1-0414F: Aerodynamic coefficients at $M = 0.3$ with free boundary layer transition.

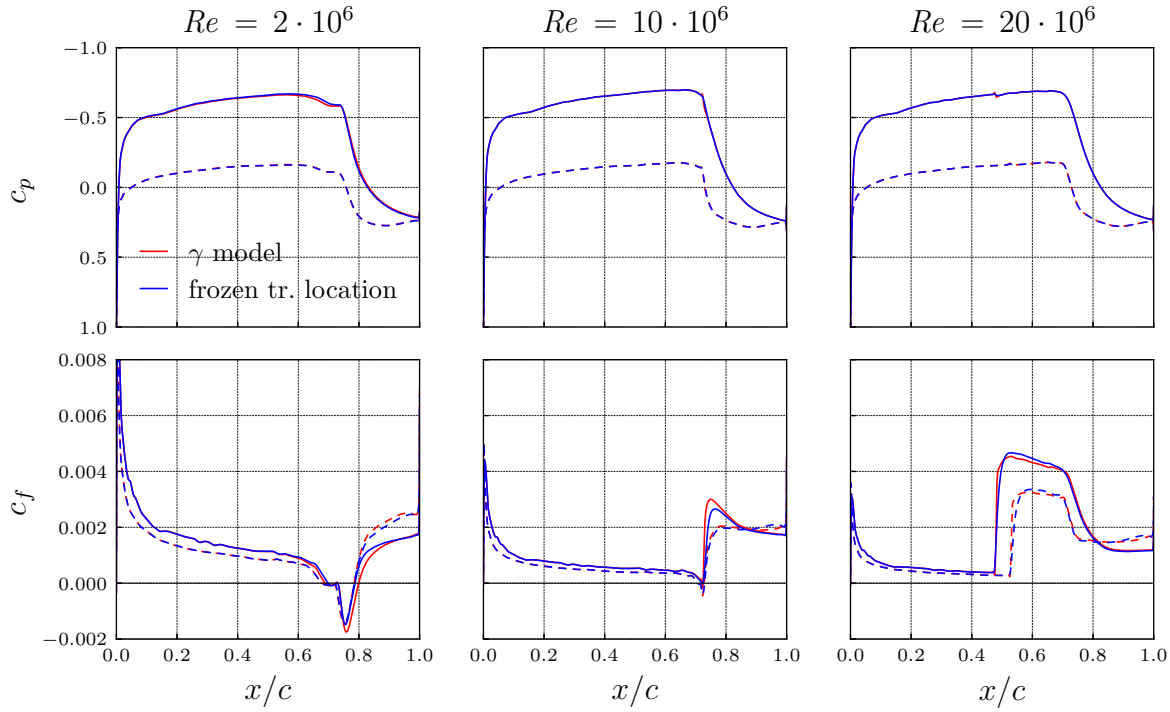

Figure 15: NLF1-0414F: Approximation of γ model results with an imposed (frozen) transition location at $\alpha = -1°$.

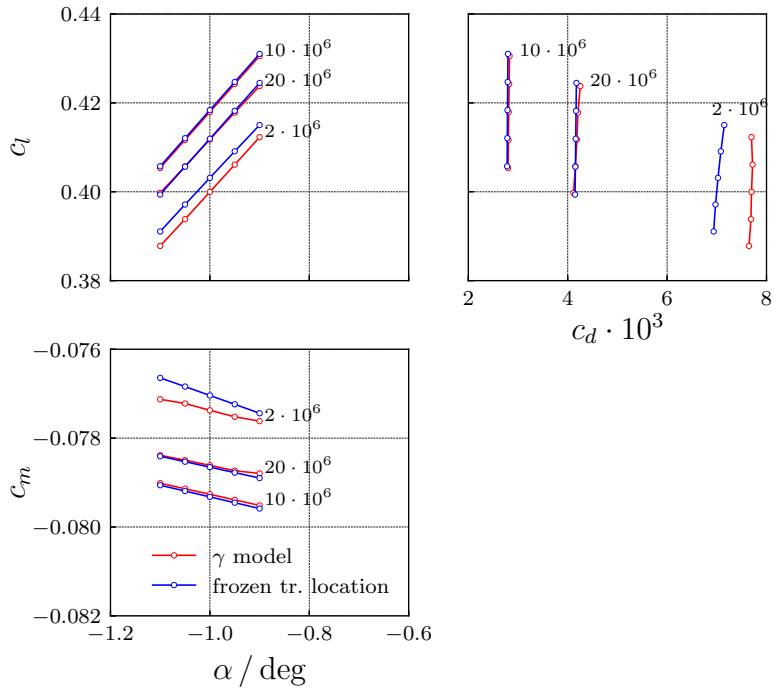

Figure 16: NLF1-0414F: Aerodynamic coefficients with corresponding Reynolds numbers.

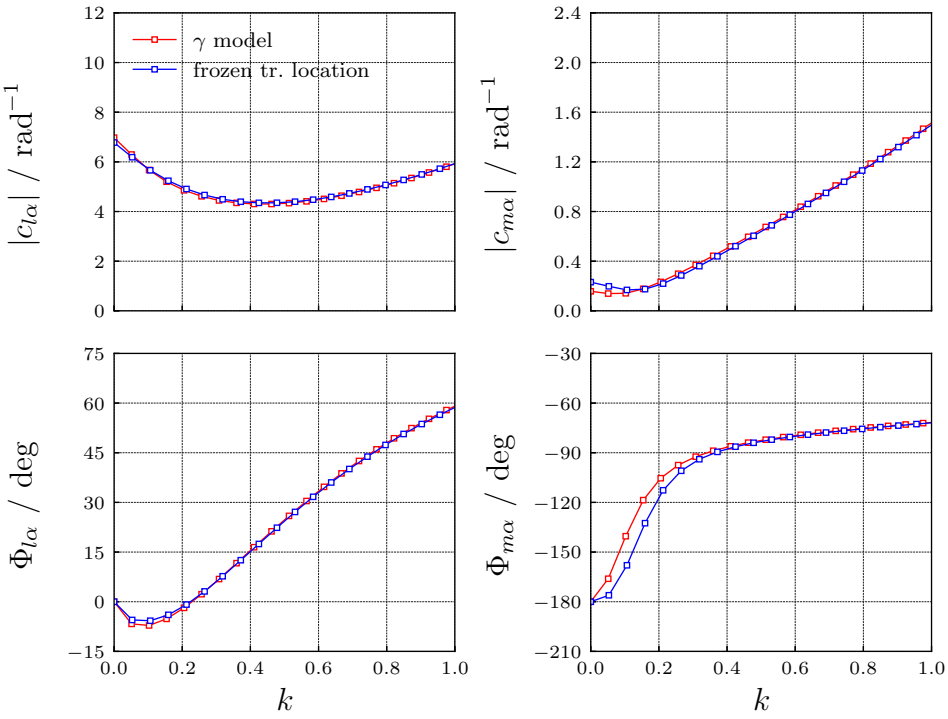

Figure 17: NLF1-0414F: Unsteady aerodynamic derivatives for a pulse excitation at $Re = 2 \cdot 10^6$.

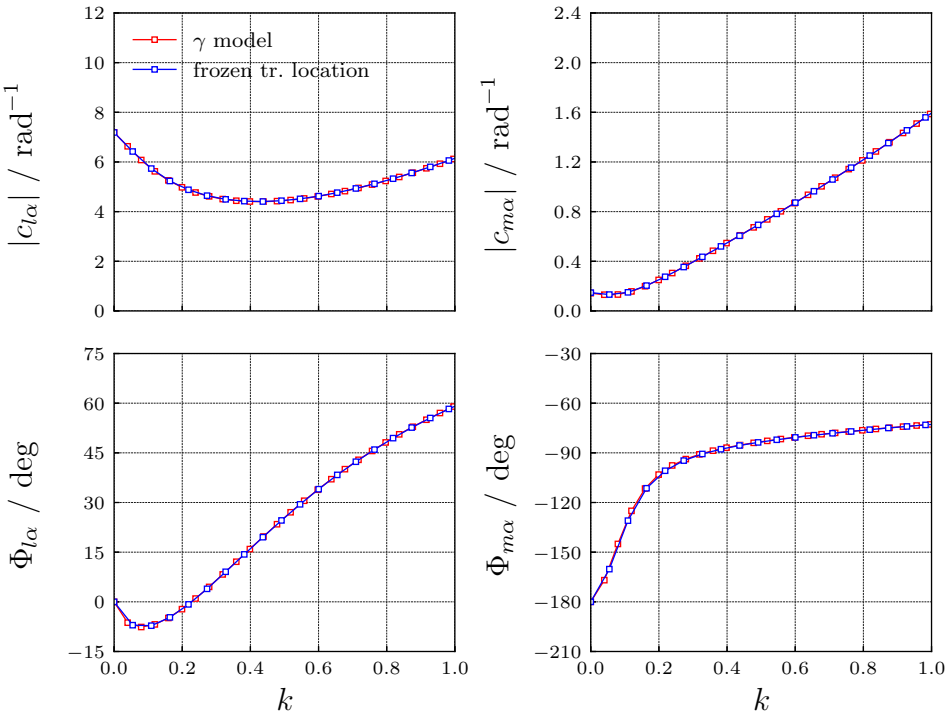

Figure 18: NLF1-0414F: Unsteady aerodynamic derivatives for a pulse excitation at $Re = 10 \cdot 10^6$.

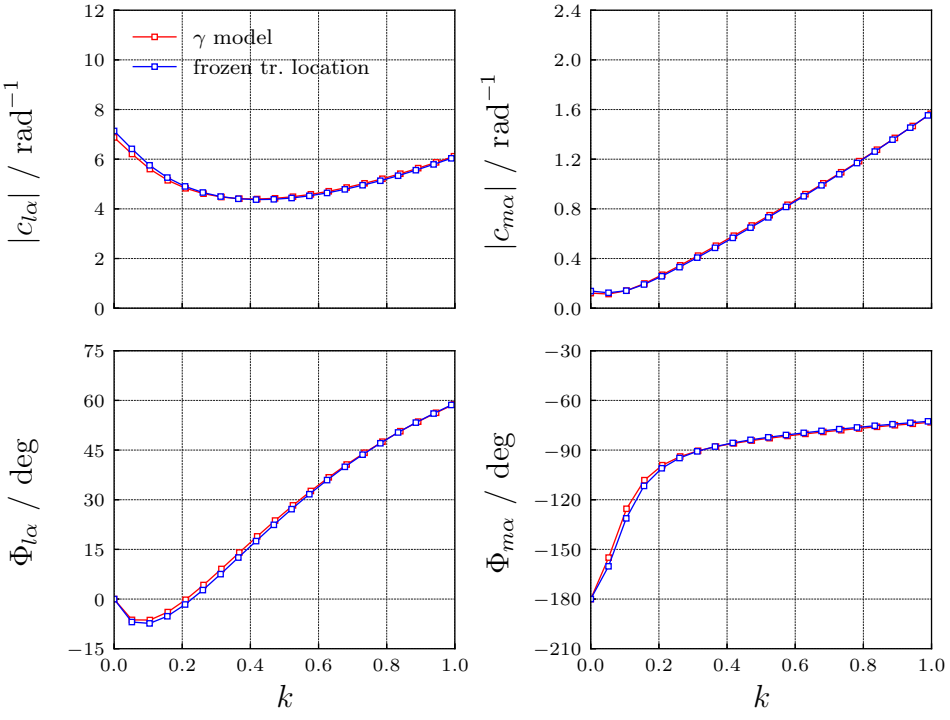

Figure 19: NLF1-0414F: Unsteady aerodynamic derivatives for a pulse excitation at $Re = 20 \cdot 10^6$.

3.3.3 NLF1-0414F: Unsteady Results

Figures 17 to 19 present the unsteady aerodynamic coefficient derivatives $c_{l\alpha}$ and $c_{m\alpha}$ for a pulse excitation in pitch. The free and the frozen transition location results for higher Reynolds numbers are virtually identical. There are minor differences at $Re = 2 \cdot 10^6$ for $k \to 0$ but these can be attributed to the different laminar-turbulent blending as a difference is already found in the steady results, see Fig. 16.

3.4 Modified SC(2)-0012: Transonic Flows at moderate to high Reynolds numbers

3.4.1 Modified SC(2)-0012: Airfoil Description

In this section, the SC(2)-0012 airfoil is used to investigate the unsteady transition behavior in transonic flow. The airfoil is part of a family of supercritical airfoils designed by NASA for transport aircraft. The 12-percent-thick symmetrical SC(2)-0012 is designed for non-lifting applications such as the vertical stabilizer [27, 28].

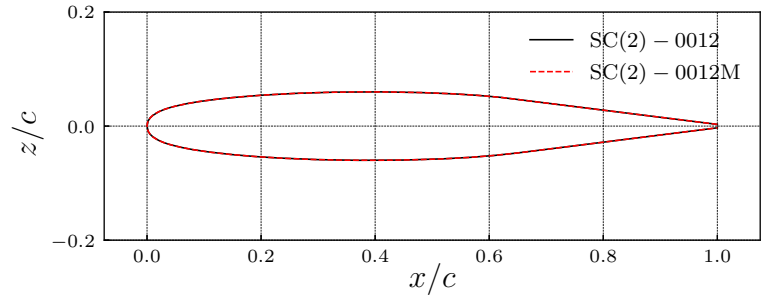

Figure 20: SC(2)-0012M: Geometry.

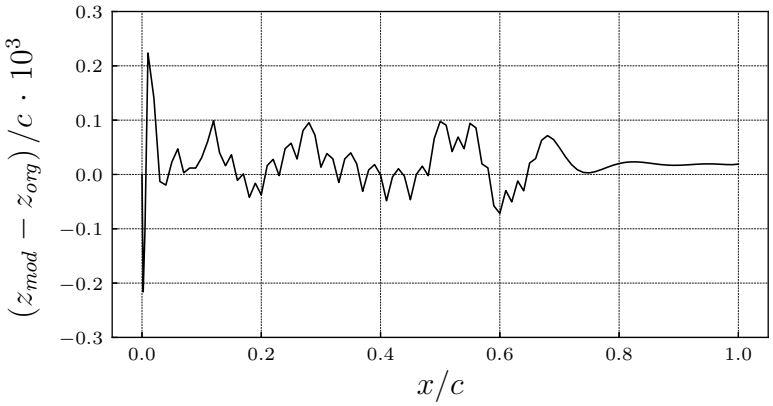

Figure 21: SC(2)-0012M: Deviation from original geometry.

The airfoil coordinates are given with 5-digit precision. The flat surface at $x/c = 0.4$ results in a wavy surface if a b-spline is used to represent the surface, which in turn results in pressure distortions that do not allow CFD computations at high Reynolds numbers. Therefore, a smoothed geometry is used, denoted as SC(2)-0012M. The original and modified airfoil are depicted in Fig. 20. The deviation from the original geometry is shown in Fig. 21.

Figure 22 shows the pressure coefficient distribution at $\alpha = 0°$, $M = 0.8$, and $Re = 20 \cdot 10^6$ computed with the γ transition model. The modified geometry gives a reasonable pressure distribution when compared to the original geometry[8].

[8]Both CFD results are well converged. Although the original and the modified airfoil are symmetric, the CFD

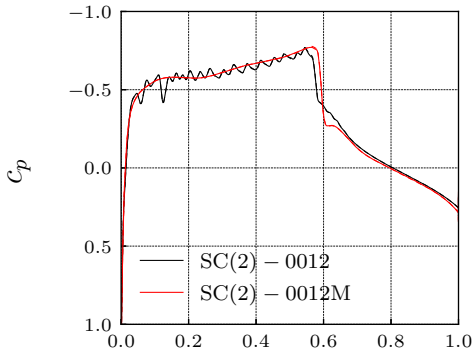

Figure 22: SC(2)-0012M: Pressure coefficient distribution at $\alpha = 0°$, $M = 0.8$, $Re = 20 \cdot 10^6$ for the original and modified airfoil.

3.4.2 Modified SC(2)-0012: Steady Results

The steady flow is computed for the SC(2)-0012M airfoil at $M = 0.8$ at different Reynolds numbers. The lift, moment, and drag coefficients are shown in Fig. 23. The slope of the lift and moment curves increase with Reynolds number as the airfoil drag decreases. There is no converged solution for $Re = 20 \cdot 10^6$ at $\alpha \geq 0.4°$. No attempt is made to obtain further results by URANS computations and thus the mean and rms error values are given. Angles of attack $\alpha > 1.4°$ for $Re = 20 \cdot 10^6$ are excluded as the flow is inherently unsteady at the given freestream conditions.

Figure 24 shows the pressure and skin friction coefficient distributions for $\alpha = 0.2°$ as obtained with the γ transition model and the TAU transition module approximation with an imposed transition location. Transition takes place at the pressure minimum on the upper and lower surface for all Reynolds numbers investigated. The boundary layer flow separates for all cases at the transition location with the exception of the lower surface at $Re = 20 \cdot 10^6$, where no laminar separation is found. The laminar separation bubble decreases in size as the Reynolds number increases.

The transition location found for $\alpha = 0.2°$ is then imposed as a frozen transition location at different angles of attack. The results for all Reynolds numbers are shown in Fig. 25. The largest offset between the free transition and the frozen transition location results are found for $Re = 10 \cdot 10^6$.

Table 2: SC2-0012M: Quasi-steady lift and moment coefficient derivatives at $\alpha = 0.2°$ for $Re = 10 \cdot 10^6$ obtained with central differences.

	$\Delta c_l \,/\, \Delta\alpha \,/$ rad^{-1}	$\Delta c_m \,/\, \Delta\alpha \,/$ rad^{-1}
γ model	15.9	−0.699
frozen intermittency	16.0	−0.718
frozen tr. location	16.7	−0.847

A frozen intermittency computation is performed in addition to the frozen transition location computation to determine the effect of the blending. Table 2 gives the quasi-steady lift and

grid is not fully symmetric, which results in small differences between the pressure distribution on the upper and lower surface.

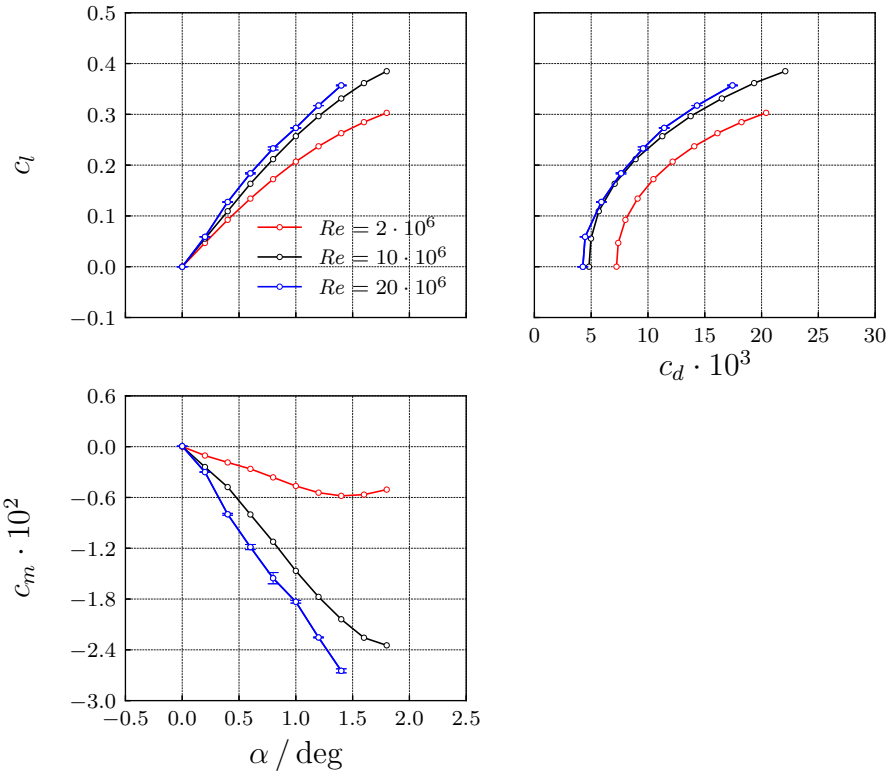

Figure 23: SC(2)-0012M: Aerodynamic coefficients at $M = 0.8$ with free boundary layer transition (γ transition model).

moment coefficient derivatives at $\alpha = 0.2°$ for $Re = 10 \cdot 10^6$ obtained with central differences based on the data given in Fig. 25. The aerodynamic coefficients for the γ transition model agree well with the frozen intermittency results once the same blending in the transition region is used.

3.4.3 Modified SC(2)-0012: Unsteady Results

Figures 26 to 28 show the unsteady aerodynamic coefficient derivatives for a pulse excitation in pitch. The results for $Re = 2 \cdot 10^6$ and $20 \cdot 10^6$ are similar for the free transition and the frozen transition location approach. There are some differences for $Re = 10 \cdot 10^6$, especially in the unsteady moment coefficient at $k \approx 0.25$ if a frozen transition location is used.

These differences are significantly reduced if the frozen intermittency field is used in the unsteady computation[9]. The different blending in the transition zone accounts for the different unsteady results given by the free transition and the frozen transition location computations. In the CAST10-2 test case by contrast, the free transition behavior is required to capture the aerodynamic resonances and the blending has only a minor effect on the unsteady results.

[9]The reason for the deviation at higher reduced frequencies is not known at the moment and might be due to a different unsteady time step size used in the computations in combination with a different pulse signal.

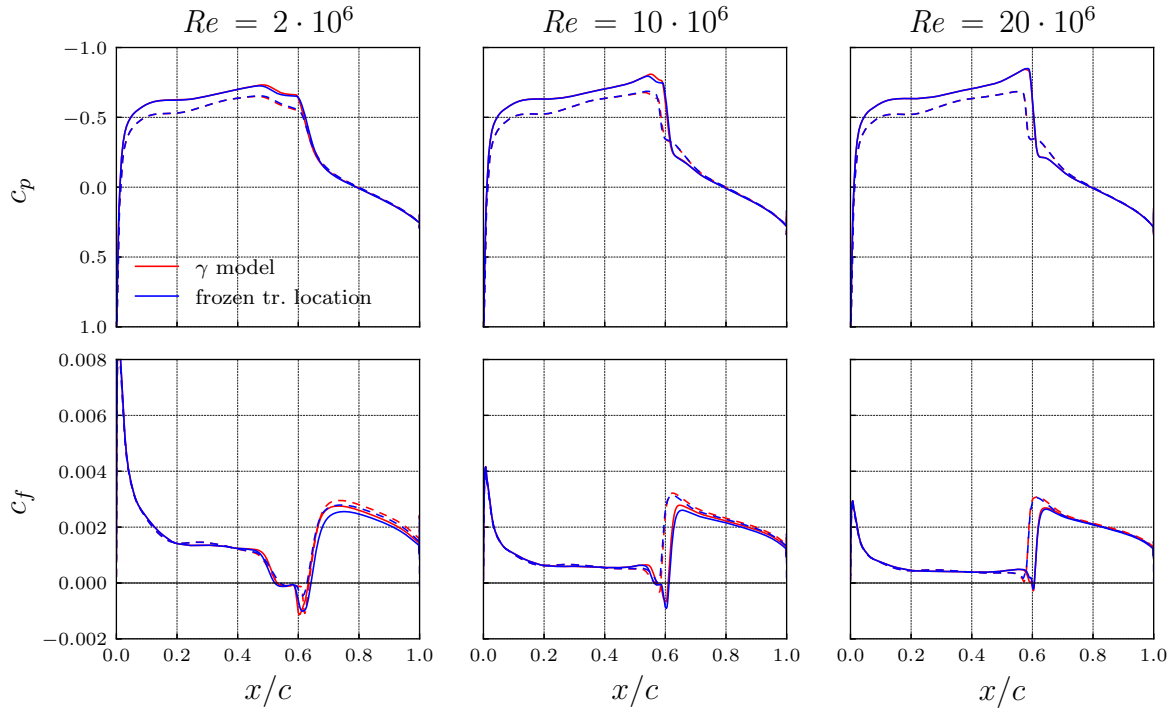

Figure 24: SC2-0012M: Approximation of γ model results by an imposed transition location at $\alpha = 0.2°$.

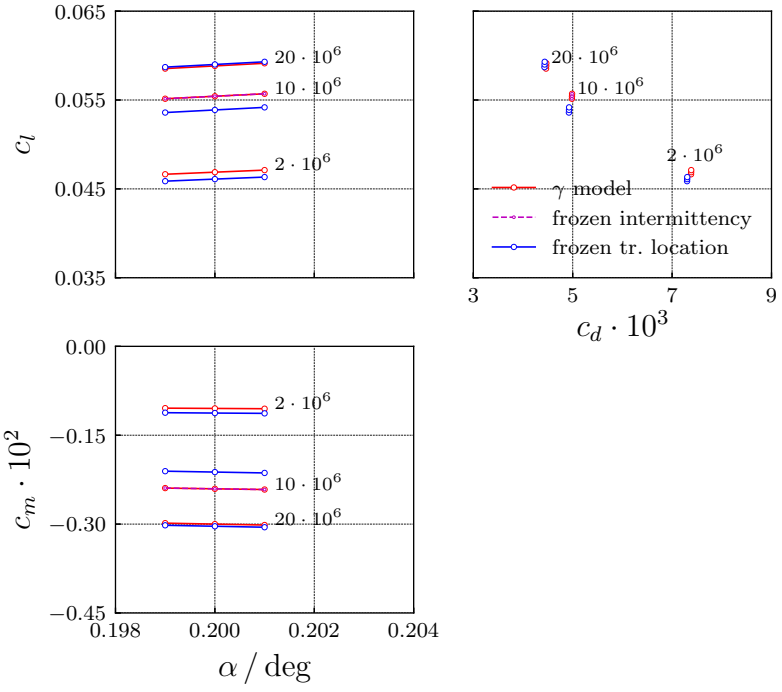

Figure 25: SC2-0012M: Aerodynamic coefficients for free and imposed transition with corresponding Reynolds numbers.

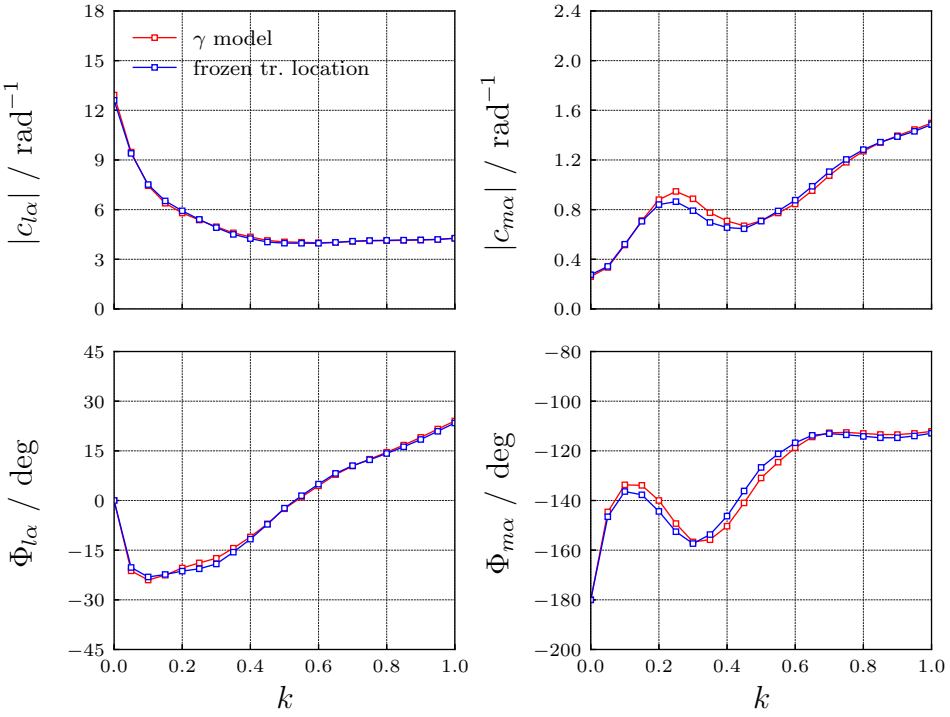

Figure 26: SC2-0012M: Unsteady aerodynamic derivatives for a pulse excitation at $Re = 2 \cdot 10^6$.

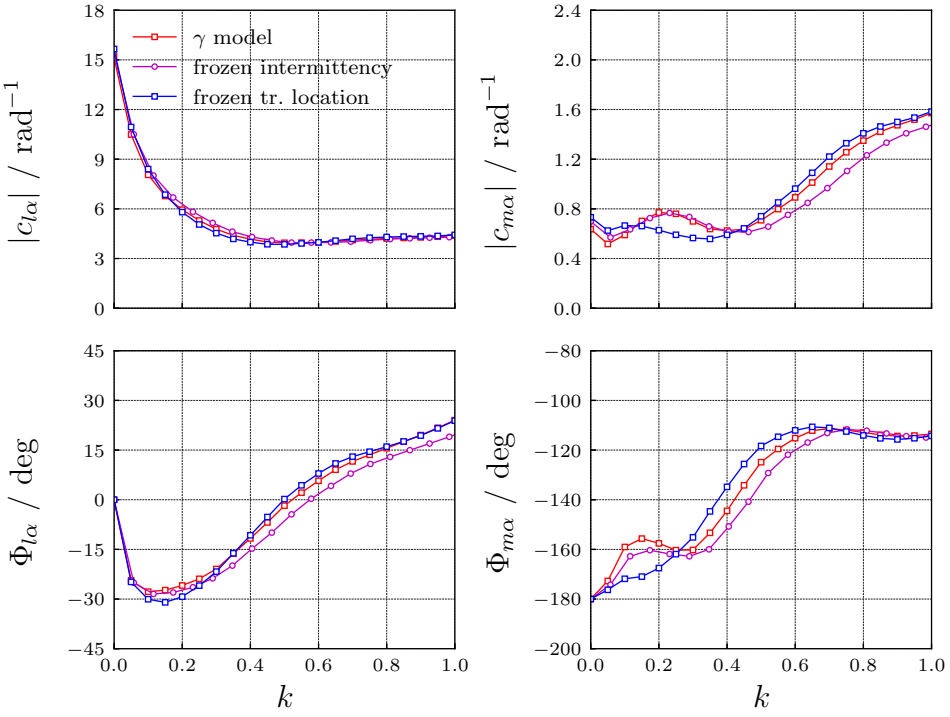

Figure 27: SC2-0012M: Unsteady aerodynamic derivatives for a pulse excitation at $Re = 10 \cdot 10^6$.

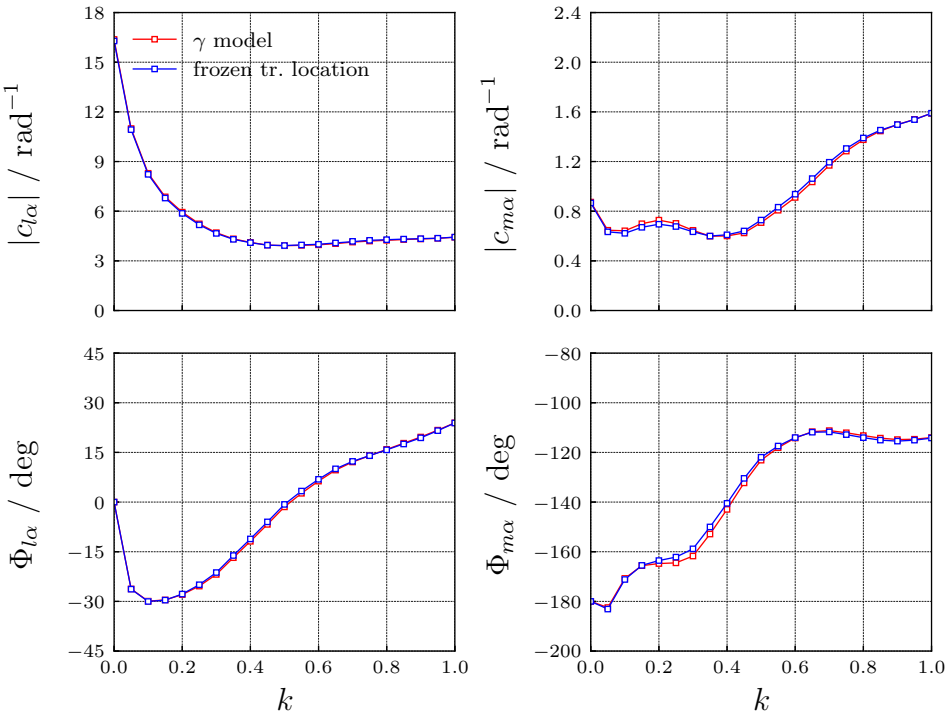

Figure 28: SC2-0012M: Unsteady aerodynamic derivatives for a pulse excitation at $Re = 20 \cdot 10^6$.

4 CONCLUSION

This paper presents steady and unsteady RANS computations for transitional flows over airfoils in a wide range of Mach and Reynolds numbers. As there are no genuine unsteady transition models that are widely accepted, the unsteady flow computations rely on the quasi-steady application of existing models. In prior investigations it was observed that certain models with free transition give the same unsteady loads as computations with a constant transition location, where the transition location remained unchanged as the numerical grid did not allow any unsteady motion of the transition location. To improve the understanding of the predicted unsteady transition behavior, a novel approach of frozen transition is introduced: the transition location is determined for the steady mean flow and this transition location (or intermittency field) is kept constant in time in an unsteady computation. This allows to determine the effect of the unsteady transition movement in a more systematic way.

The Reynolds number has a first-order effect on the transition location: the transition location moves upstream with increasing Reynolds number for a constant disturbance environment. In addition, the pressure distribution is usually affected by a change in Reynolds number as e.g. the separation behavior of the laminar boundary layer is altered. Any change in pressure gradient will alter the transition location as well. Both effects aggravate the difficulties to trace transitional effects over a broad Reynolds number range. In general, it can be stated that the approximation of the unsteady aerodynamics with free boundary layer transition by a frozen transition approach improves with increasing Reynolds number. At the moment, there is no specific threshold Reynolds number above which a steady approach is sufficient.

Unsteady flow conditions for which the frozen transition location or intermittency field give a good quasi-steady approximation of the aerodynamics, are likely to be captured with the frozen transition assumption. However, resonance phenomena as found for the CAST10-2 depend

highly on the unsteady transition behavior and need to be captured by an appropriate transition model. Although effects of similar severity have not been observed at free-flight Reynolds numbers, they cannot be dismissed.

The NLF1-0414F airfoil in subsonic flow does not show a significant effect if free transition results are compared to frozen transition location results. This is rather surprising as one might expect an inclination towards unsteady flow behavior in the case of large laminar separations or for transition in a favorable pressure gradient region. Future investigations will show if a transitional, subsonic flow can experience a transition-induced resonance behavior similar to that observed in transonic flows in the presence of shocks.

The low Reynolds number results for the CAST10-2 airfoil show that the modeling of the transition zone has already a strong influence on the steady flow field. Although the approximation of the γ model's transition location by the TAU transition module is reasonable, the downstream development of the boundary layer results in rather large differences in the values of the aerodynamic coefficients. In addition, this observation underlines the difficulties to match experimental data as a good agreement in the transition location does not necessarily produce a good agreement in the aerodynamic coefficients even at steady flow conditions.

Future transition models need to improve the model behavior inside the transition zone. The transition process itself is an unsteady and three-dimensional phenomenon, although the overall flow conditions on a larger scale might be steady. This raises the question if an appropriate representation within the framework of a RANS model is feasible. In theory, it should be possible to define an intermittency field within a transition model that gives a representation of the intermittency factor measured in an experiment. The intermittency factor should provide the blending from a laminar to a turbulent boundary layer, but it should also be descriptive in terms of physical quantities inside the transition zone, as the development of the displacement thickness over the transition zone is essential for the prediction of the aerodynamic behavior. In addition, further validation data in a broad frequency range at different mean flow conditions is required to improve existing transition models or to develop and validate unsteady transition models.

5 REFERENCES

[1] Fehrs, M. (2018). Boundary Layer Transition in External Aerodynamics and Dynamic Aeroelastic Stability. Dissertation, Technical University Braunschweig, ISSN 1434-8454, ISRN DLR-FB-2018-11, also NFL-FB 2017-27, Braunschweig, Germany.

[2] Tichy, L., Mai, H., Fehrs, M., Nitzsche, J., Hebler, A. (2017). Risk Analysis for Flutter of Laminar Wings. IFASD, IFASD-2017-196, Como, Italy.

[3] Helm, S., Fehrs, M., Nitzsche, J. (2018). CFD-based Aeroelastic Analysis of NLF Wings. STAB, 21. DGLR Fachsymposium der STAB, Darmstadt, Germany.

[4] Betchov, R., Criminale, Jr., W. O. (1967). Stability of Parallel Flows. *Applied Mathematics and Mechanics* edited by F. N. Frenkiel, G. Temple, 10, New York: Academic Press.

[5] Hassig, H. J. (1971). An Approximate True damping Solution of the Flutter Equation by Determinant Iteration. *Journal of Aircraft*, 8(11), pp. 885–889.

[6] Kaiser, C., Thormann, R., Dimitrov, D., Nitzsche, J. (2015) Time-Linearized Analysis of Motion-Induced and Gust-Induced Airloads with the DLR TAU Code. *Deutscher Luft- und Raumfahrtkongress 2015*, Rostock, Germany.

[7] van Ingen, J. L. (1956). A Suggested Semi-Empirical Method for the Calculation of the Boundary Layer Transition Region. *Technische Hogeschool Vliegtuigbouwkunde*, Report V.T.H.-74, Delft, Netherlands.

[8] Smith, A. M. O., Gamberoni, N. (1956). Transition, Pressure Gradient and Stability Theory. Douglas Aircraft Company, Report ES 26388, El Segundo, USA.

[9] van Ingen, J. L. (2008). The e^N Method for Transition Prediction. Historical Review of Work at TU Delft. 38^{th} *Fluid Dynamics Conference and Exhibit*, AIAA 2008-3830, Seattle, USA.

[10] Krumbein, A., Krimmelbein, N., Schrauf, G. (2009). Automatic Transition Prediction in Hybrid Flow Solver, Part 1: Methodology and Sensitivities. *Journal of Aircraft*, 46(4), pp. 1176–1190.

[11] Krumbein, A., Krimmelbein, N., Schrauf, G. (2009). Automatic Transition Prediction in Hybrid Flow Solver, Part 2: Practical Application. *Journal of Aircraft*, 46(4), pp. 1191–1199.

[12] Menter, F. R., Langtry, R. B., Likki, S. R., Suzen, Y. B., Huang, P. G., Völker, S. (2006). A Correlation-Based Transition Model Using Local Variables – Part I: Model Formulation. *Journal of Turbomachinery*, 128(3), pp. 413–422.

[13] Langtry, R. B., Menter, F. R., Likki, S. R., Suzen, Y. B., Huang, P. G., Völker, S. (2006). A Correlation-Based Transition Model Using Local Variables – Part II: Test Cases and Industrial Applications. *Journal of Turbomachinery*, 128(3), pp. 423–434.

[14] Langtry, R. B. and Menter, F. R. (2009). Correlation-Based Transition Modeling for Unstructured Parallelized Computational Fluid Dynamics Codes. *AIAA Journal*, 47(12), pp. 2894–2906.

[15] Dick, E., Kubacki, S. (2017). Transition Models for Turbomachinery Boundary Layer Flows: A Review. *International Journal of Turbomachinery, Propulsion ans Power*, MDPI, 2(4).

[16] Neumann, J., Friedewald, D., Hennings, H. (2018). The Influence of Fixed Transition Modeling on Aeroelastic Simulations in Comparison to Wind Tunnel Experiments. *CEAS Aeronautical Journal*, 9(3), pp 491–503.

[17] Stanewsky, E., Zimmer, H. (1980). Development and Wind Tunnel Investigation of Three Supercritical Airfoil Profiles for Transport Aircraft. NASA, TM-75840, Washington, D.C., USA.

[18] Dress, D. A., Johnson, C. B., McGuire, P. D., Stanewsky, E., Ray, E. J. (1983). High Reynolds Number Tests of the CAST 10-2/DOA 2 Airfoil in the Langley 0.3-Meter Transonic Cryogenic Tunnel - Phase I. NASA, TM-84620, Hampton, USA.

[19] Mai, H., Hebler, A. (2011). Aeroelasticity of a Laminar Wing. In: Proc. *International Forum on Aeroelasticity and Structural Dynamics*, IFASD, 2011-128, Paris, France.

[20] Hebler, A., Schojda, L., Mai, H. (2013). Experimental Investigation of the Aeroelastic Behavior of a Laminar Airfoil in Transonic Flow. In: Proc. *International Forum on Aeroelasticity and Structural Dynamics*, IFASD, 32C, Bristol, UK.

[21] van Rooij, A. C. L. M., Wegner, W. (2014). Numerical Investigation of the Flutter Behaviour of a Laminar Supercritical Airfoil. In: *New Results in Numerical and Experimental Fluid Mechanics IX*, edited by Dillmann, A. et al., Cham: Springer, pp. 33–41.

[22] Fehrs, M., van Rooij, A. C. L. M., Nitzsche, J. (2015). Influence of Boundary Layer Transition on the Flutter Behavior of a Supercritical Airfoil. *CEAS Aeronautical Journal*, 6(2), pp. 291–303.

[23] Hebler, A. (2017). Experimental Assessment of the Flutter Stability of a Laminar Airfoil in Transonic Flow. In: Proc. *International Forum on Aeroelasticity and Structural Dynamics*, IFASD, 2017-089, Como, Italy.

[24] Braune, M., Hebler, A. (2018). Experimental Investigation of Transonic Flow Effects on a Laminar Airfoil Leading to Limit Cycle Oscillations. *2018 Applied Aerodynamics Conference*, AIAA AVIATION Forum, AIAA 2018-3641, Atlanta, USA.

[25] Braune, M., Hebler, A. (2019). Mechanisms of Transonic Single Degree of Freedom Flutter of a Laminar Airfoil. In: Proc. *International Forum on Aeroelasticity and Structural Dynamics*, IFASD, 2019-132, Savannah, USA.

[26] McGhee, R. J., Viken, J. K., Pfenninger, W., Beasley, W. D., Harvey, W. D. (1984). Experimental Results for a Flapped Natural-Laminar-Flow Airfoil with High Lift/Drag Ratio. NASA, TM-85788, Hampton, USA.

[27] Mineck, R. E., Lawing, P. L. (1987). High Reynolds Number Tests of the NASA SC(2)-0012 Airfoil in the Langley 0.3-Meter Transonic Cryogenic Tunnel. NASA, TM-89102, Hampton, USA.

[28] Harris, C. D. (1990). NASA Supercritical Airfoils. NASA, TP-2969, Hampton, USA.

COPYRIGHT STATEMENT